Hyperfine Interact (2016) 237:81
DOI 10.1007/s10751-016-1286-5

Sensitivity of ^{57}Fe emission Mössbauer spectroscopy to Ar and C induced defects in ZnO

K. Bharuth-Ram[1] · T. E. Mølholt[2] · G. Langouche[3] · S. Geburt[4] · C. Ronning[4] · T. B. Doyle[5,6] · H. P. Gunnlaugsson[2] · K. Johnston[2] · R. Mantovan[7] · H. Masenda[8] · D. Naidoo[8] · M. Ncube[8] · H. Gislason[9] · S. Ólafsson[9] · G. Weyer[10]

Abstract Emission Mössbauer Spectroscopy (eMS) measurements, following low fluence ($<10^{12}$ cm^{-2}) implantation of ^{57}Mn ($t_{1/2}$ = 1.5 min.) into ZnO single crystals pre-implanted with Ar and C ions, has been utilized to test the sensitivity of the ^{57}Fe eMS technique to the different types of defects generated by the different ion species. The dominant feature of the Mössbauer spectrum of the Ar implanted ZnO sample was a magnetic hyperfine field distribution component, attributed to paramagnetic Fe^{3+}, while that of the

This article is part of the Topical Collection on *Proceedings of the International Conference on the Applications of the Mössbauer Effect (ICAME 2015), Hamburg, Germany, 13-18 September 2015*

✉ K. Bharuth-Ram
kbr@tlabs.ac.za

1 School of Physics, Durban University of Technology, Durban 4000, South Africa

2 PH Department, ISOLDE/CERN, 1211 Geneva 23, Geneva, Switzerland

3 Instituut voor Kern-en Stralingsfysica, KU Leuven, University of Leuven, B-3001 Leuven, Belgium

4 Institute for Solid State Physics, Friedrich-Schiller University of Jena, Jena, Germany

5 iThemba LABS, Somerset West 7129, Western Cape Province, South Africa

6 School of Chemistry and Physics, University of KwaZulu-Natal, Durban 4000, South Africa

7 Laboratorio MDM, IMM-CNR, Via Olivetti 2, I-20864 Agrate Brianza MB, Italy

8 School of Physics, University of the Witwatersrand, Johannesburg, WITS 2050, South Africa

9 Science Institute, University of Iceland, Dunhaga 3, IS-107 Reykjavík, Iceland

10 Department of Physics and Astronomy, University of Aarhus, Aarhus, Denmark

Published online: 14 March 2016

C implanted sample was a doublet attributed to substitutional Fe^{2+} forming a complex with the C dopant ions in the 2^- state at O vacancies. Magnetization measurements on the two samples, on the other hand, yield practically identical m(H) curves. The distinctly different eMS spectra of the two samples display the sensitivity of the probe nucleus to the defects produced by the different ion species.

Keywords ZnO · Ar and C implantation · Emission Mössbauer Spectroscopy · Defect sensitivity

1 Introduction

Research focus on magnetism in doped ZnO has shifted from intrinsic to extrinsic effects; in particular on the role of defects in the observed effects and in their possible utilization to tailor the physical properties of ZnO to particular applications [1, 2]. This requires knowledge of the different types of defects that are formed by different ion types. In general, lattice defects formed in crystalline substrates are followed by Rutherford backscattering spectrometry in Channeling configuration [see, for example, ref. [3]] Other techniques, such as electron paramagnetic resonance (EPR) [4], X-ray diffraction (XRD) and particle induced X-ray emission (PIXE) analysis, have also yielded information on irradiation induced defects. In the present contribution we explore the sensitivity of ^{57}Fe emission Mössbauer Spectroscopy (eMS) following the implantation of radioactive parent $^{57}Mn^+$ ions, to implantation-induced defects in ZnO. As test systems we have selected two ZnO single crystal samples, one implanted with ^{40}Ar – an inert gas atom that produces vacancies and interstitials but does not form any complex with atoms of the substrate or of the probe ion; the other implanted with ^{12}C ions which are reported to form ZnO-C bonds in the ZnO matrix [5].

2 Experimental

As systems for our eMS study, we selected three ZnO single crystal samples. One was pre-implanted with 45 keV ^{40}Ar ions to a fluence of 4.5×10^{15} cm^{-2}. The other two pre-implanted with 15 keV ^{12}C ions to a fluences of 1.2×10^{16} cm^{-2} and 3.0×10^{15} cm^{-2}, corresponding to peak concentrations of 4 at.% and 1 at.%, respectively. The implantation energies were chosen so that the implantation profiles of the Ar and C ions matched that of 50 keV ^{57}Mn beam available at ISOLDE/CERN. Simulations of the implantation profiles, using the Monte Carlo code SRIM [6], are shown in Fig. 1 where for illustrative purposes the ^{57}Mn distribution is multiplied by a factor of 10^3. The simulations predict nearly Gaussian Mn, Ar and C distributions, only slightly skewed, centred at a depth of 30(2) nm and with a straggle of 14(1) nm. SRIM simulations (Fig. 2) predicted the implantation generated damage -vacancies and interstitials- to extend from the surface to 70 nm depth, peaking around 30 nm, with ∼40 % more Zn vacancies and interstitials than O defects of the same type.

^{57}Mn ions were produced at the ISOLDE facility at CERN using 1.4 GeV proton induced fission in a UC_2 target and element selective laser ionization. The mass separated Mn ions were accelerated to 50 keV and implanted into the pre-implanted ZnO single crystal samples at 30°relative to the sample normal, at a rate of few times 10^8 ions/s. With a beam diameter

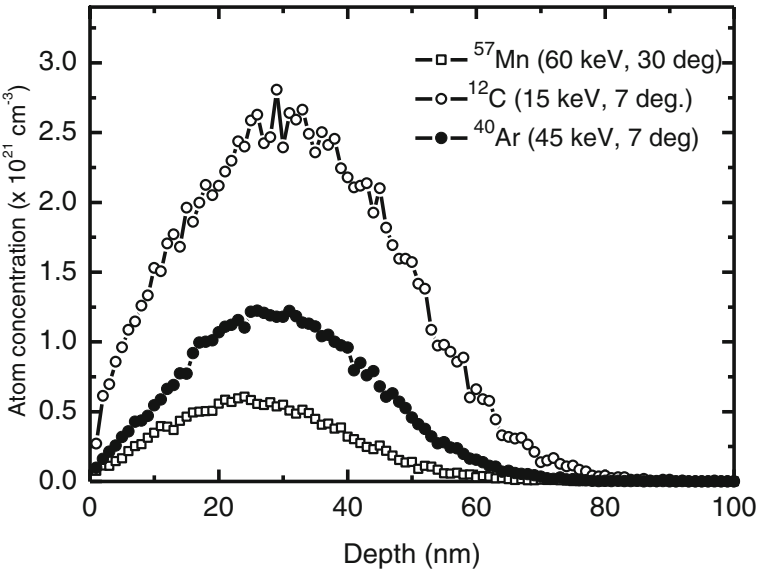

Fig. 1 SRIM simulations of the concentration profiles of ^{40}Ar, ^{12}C, and ^{57}Mn implanted in ZnO with implantation parameters shown. For illustrative purposes the ^{57}Mn concentration has been multiplied by a factor of 1000

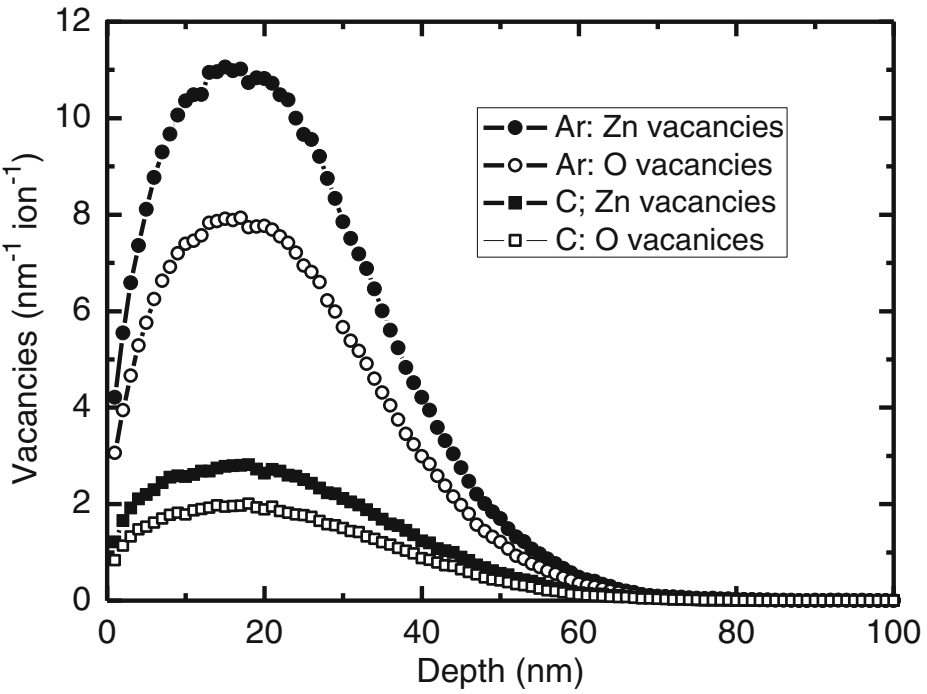

Fig. 2 SRIM simulations of the Zn and O vacancy distributions produced by the Ar and C ions

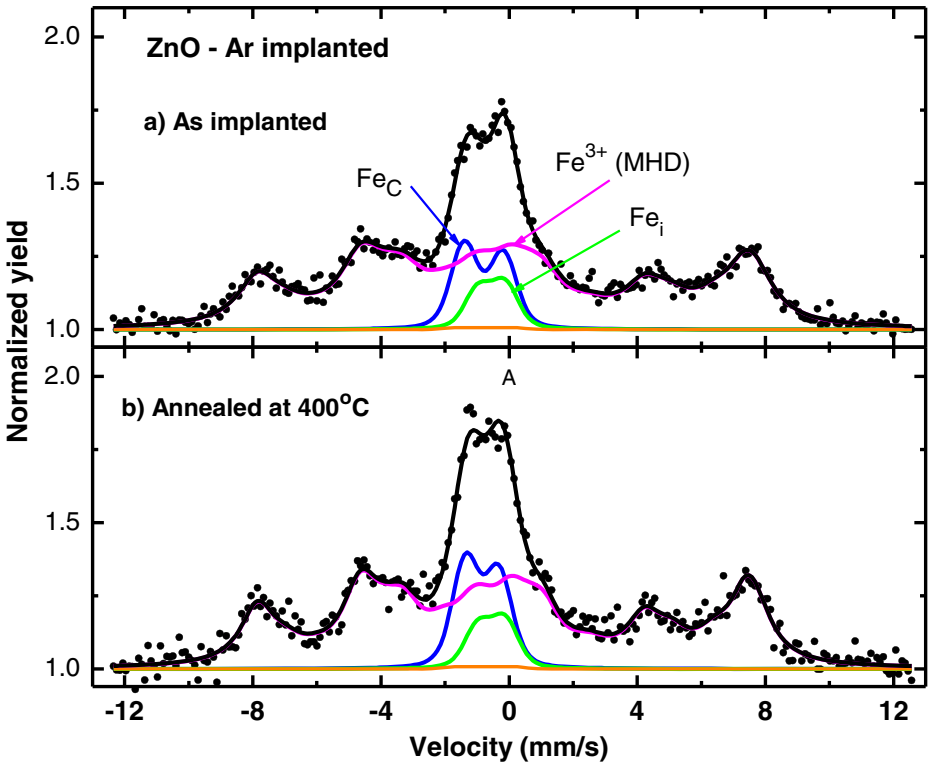

Fig. 3 Room temperature ^{57}Fe emission Mössbauer spectra of the Ar pre-implanted ZnO single crystal, together with the spectral components required to fit the data: **a**) As-implanted, and **b**) after annealing for 15 min. at 400°C

of 6 mm and a fluence rate of the order ~10^9 ^{57}Mn/(cm^2•s), the total implanted fluence was less than 2×10^{12} ions/cm^2 (concentration $\sim 10^{-4}$ at.%)

Emission Mössbauer spectra were measured at room temperature (RT) on-line during implantation using a parallel plate avalanche detector equipped with a stainless steel electrode enriched in ^{57}Fe as absorber. The detector was mounted 60° relative to the sample normal (90 ° relative to the beam). Isomer shifts and velocities were calibrated relative to the spectrum of α-Fe at RT.

Magnetization measurements were made on the samples after the eMS measurements, with a vibrating sample magnetometer with a sensitivity of 10^{-6} emu (incorporated in a Cryogenics PPMS system).

3 Results and analysis

The RT emission Mössbauer spectra of the Ar implanted ZnO sample, as-implanted and after annealing at 400°C for 15 min. in vacuum, are shown in Fig. 3a and b. Based on

Table 1 Hyperfine parameters, isomer shift (δ), quadrupole splitting (ΔE_Q), the highest magnetic hyperfine field of the MHD (B_{hf}) and the Gaussian broadening (σ) and areal fractions (A) extracted from a simultaneous fit to the spectra Ar implanted ZnO shown in Fig. 3

	Component	δ (mm/s)	ΔE_Q (mm/s)	B_{hf} (T)	σ (mm/s)	A (%)	Assignment
As implanted	D1	0.79(3)	−1.22(3)	–	0.34(2)	14(1)	$Fe^{2+}{}_{Zn}$
	D2	0.55	+0.85	–	0.33(5)	7	Fe_i
	D3	0.77	1.3	–	0.8	<1	Fe_D
	MHD			46.8		79(3)	Fe^{3+}
Annealed at 400°C	D1	0.84(3)	−1.0(3)	–	0.34(3)	16(1)	$Fe^{2+}{}_{Zn}$
	D2	0.55	+0.85	–	0.33(5)	7	Fe_i
	D3	0.77	1.3	–	0.8	<1	Fe_D
	MHD			46.8		77(3)	Fe^{3+}

(Note: Parameter values shown without error were kept fixed in the analysis.)

our earlier studies [7, 9] the spectra were analyzed in terms of four components: three doublets, and a magnetic hyperfine field distribution (MHD) due to paramagnetic Fe^{3+} [10]. The doublets are assigned to Fe^{2+} at substitutional Zn sites (Fe_C) [7], Fe in interstitial sites (Fe_i) and Fe in implantation induced lattice defects (Fe_D). The doublets were analyzed with spectral components with Voigt line shapes with an instrumental Lorentzian line width $\Gamma = 0.34$ mm/s and Gaussian broadening $\sigma = 0.08$ mm/s determined from the calibration spectrum. The fit parameters are listed in Table 1 The magnetic component dominates the spectrum, which with an area fraction of 79(3)% for the asimplanted sample, is slightly stronger than observed in eMS study of $^{57}Mn/^{57}Fe$ implanted in virgin ZnO [7], but in agreement with the fraction observed in eMS measurements on Na-implanted ZnO at saturation fluences [11].

The dominating MHD component makes it difficult to obtain a unique analysis of the central part of the spectra. Hence, in order to obtain a consistent analysis of the data, the hyperfine parameters of interstitial Fe and Fe in damage sites were therefore kept fixed at values determined in our earlier studies [7, 8] and only the substitutional fraction was allowed to be freely fitted. The annealing at 400°C (Fig. 4b) evidently produces minor change to the spectrum (and of the defects created by the Ar implantation) except for a decrease in the quadrupole splitting of the substitutional Fe^{2+} component.

The RT spectra of the ZnO samples implanted with 1 and 4 at. % C ions are presented in Fig. 4 and are analyzed in a similar way as discussed above. The spectra show no evidence of a magnetic Fe^{3+} component, and instead, are dominated by a doublet with isomer shift and quadrupole splitting values consistent (Table 2) with those of Fe^{2+} at substitutional Zn sites [7]. Small contributions of a doublet due to Fe in interstitial sites with fixed parameters ($\delta = 0.77$ mm/s, $\Delta E_Q = 0.85$ mm/s), has been included in the analysis. It is not possible to distinguish between a possible damage component and the dominating substitutional Fe^{2+} component. Including a possible damage component as described in Table 1 and [8] (less than 1% area fraction) results in a similar good fit to the data.

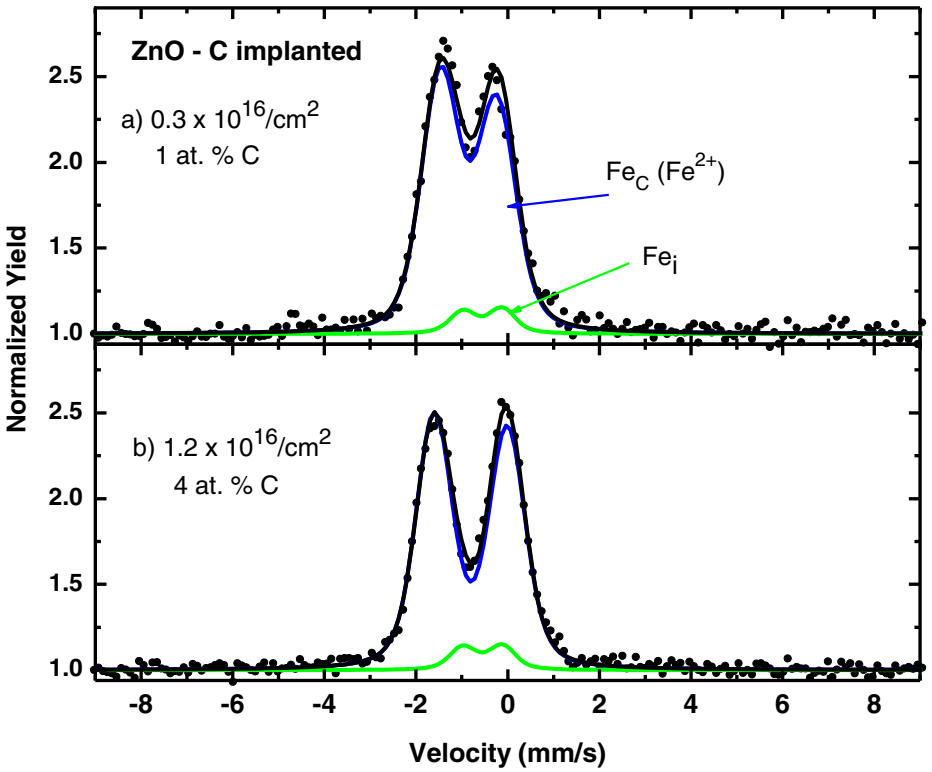

Fig. 4 Room temperature ^{57}Fe emission Mössbauer spectra of ZnO single crystal samples pre-implanted with C ions to a fluence of **a**) $1.2{\cdot}10^{16}$ ions/cm^2 and **b**) $3.0{\cdot}10^{15}$ ions/cm^2

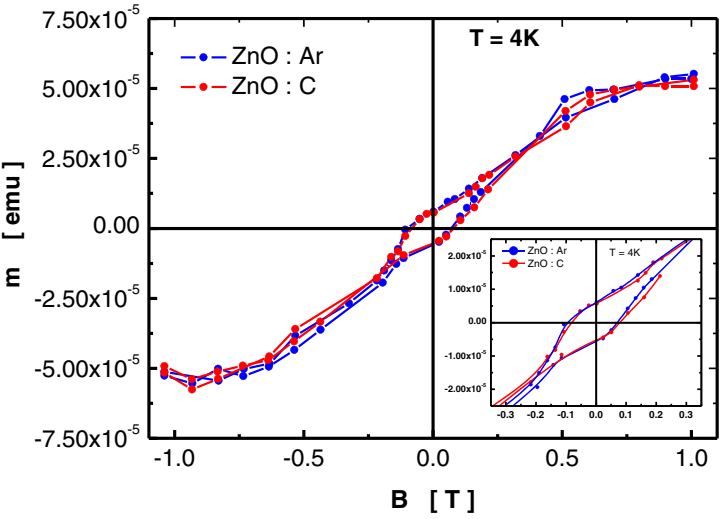

Fig. 5 Magnetization curves of the Ar and C implanted ZnO samples, measured at 4 K

Table 2 Isomer shift (δ), quadrupole splitting (ΔE_Q), additional Gaussian broadening (σ) and areal fractions (A) extracted from a simultaneous fit to the spectra of C implanted ZnO shown in Fig. 4

	Component	δ (mm/s)	ΔE_Q (mm/s)	σ (mm/s)	A (%)	Assignment
1 at. % C	D1	0.85(1)	1.23(1)	0.34(1)	93(2)	Fe^{2+}
	D2	0.55	0.85	0.21	7(2)	Fe_i
4 at. % C	D1	0.80(1)	1.60(1)	0.31(1)	95(2)	Fe^{2+}
	D2	0.55	0.85	0.21	5(1)	Fe_i

(Note: Parameter values shown without error were kept fixed in the analysis.)

The increase in quadrupole splitting of the substitutional Fe^{2+} component with increased carbon implantation fluence is consistent with what has been observed previously [12] and indicative of an increase in lattice damage creating less perfect substitutional sites.

Finally in Fig. 5 we present the magnetization vs. applied field, m(H), curves obtained from the VSM measurements at 4 K, conducted after the eMS measurements. Both samples show practically identical magnetic behavior with the suggestions of small hysteresis effects. The magnitude of the magnetization points on the curves, however, is approaching the limiting sensitivity/noise level of the magnetometer.

4 Discussion

There are several earlier studies of Ar implanted ZnO. Adekore *et al* [13] studied the annealing behavior of defects in ZnO produced by Ar implantation, using several interrogation techniques, and reported that crystallographic repair sets in at 400°C annealing. Ferromagnetic behaviour in Ar implanted ZnO has been reported by both Borges *et al* [14] and Mishra *et al* [15], but at fluences above 1.5×10^{16} Ar ions/cm^2. Both authors assign the observed effects to oxygen vacancies created by the implanted Ar ions which make no contribution to the magnetism.

In our case, it is evident from the magnetization measurements (Fig. 5) that the Ar implantation has produced no clear signature of stable ferromagnetic order in the ZnO sample, indicating that the effects evident in the eMS spectra (Fig. 3) have a similar origin as reported in our earlier study [7, 9, 10], i.e. due to the Fe produced in the ^{57}Mn β-decay being trapped as paramagnetic Fe^{3+} centres in implantation induced defects. The SRIM simulations (Fig. 2) show that approx. 40% more Zn vacancies than O vacancies are produced by the Ar (and C) ions. However, Zn interstitials are fast diffusers with a low migration barrier [16]. Their recombination with Zn vacancies would considerably reduce the latter, resulting in an order of magnitude higher oxygen vacancies [15]. Hence we may attribute the observed magnetic features in the spectra to Fe^{3+} on substitutional Zn sites interacting with oxygen vacancies.

Carbon implanted ZnO thin films have also been reported to show room temperature ferromagnetism (RTFM) at dopant concentrations of 1 at% and higher [5, 17, 18]. Zhou *et al*, in a comparative study with Ne implanted ZnO, show that the RTFM observed in C implanted ZnO is due to the chemical involvement of the C ions. *Ab initio* Density Functional Theory (DFT) study of Pham *et al*. [19] yield the result that the dominant state of C in ZnO is C in the O-vacancy where it is in the 2− charge state, i.e. C_O^{2-}. The absence of any evidence of ferromagnetism or of paramagnetic Fe^{3+} centres in our eMS data is consistent

with this scenario which would lead to the Fe ions in the Fe^{2+} state coupling with the C_O^{2-} and thereby cancelling any spin alignment.

5 Conclusions

We have conducted ^{57}Fe-emission Mössbauer spectroscopy measurements following the low fluence ($<10^{12}$ cm^{-2}) implantation of ^{57}Mn into ZnO single crystal samples pre-implanted with Ar and C ions. The implanted ions behave differently in the ZnO matrix. The inert Ar form no coupling with the Zn or O ions, but play a major role in the creation of lattice defects. The C ions, on the other hand, couple to O vacancies. At the low concentration levels used in our study both the Ar- and C-implanted ZnO samples display practically identical magnetisation behaviour. The emission Mössbauer spectra of the two samples, however, are distinctly different, attesting to the extreme sensitivity of the ^{57}Fe-eMS technique to the different types of defects created by the different ion species.

Acknowledgments This work was supported by the South African National Research Foundation and the Department of Science and Technology, the Deutsche Forschungsgemeinschaft (Contract no. Ro1198/13-1) and the European Union Seventh Framework through ENSAR (Contract no. 262010). R. Mantovan acknowledges support from MIUR through the FIRB Project RBAP115AYN "Oxides at the nanoscale: multifunctionality and applications". T. E. Mølholt and S. Olafsson acknowledge support from the Icelandic Research Fund.

References

1. Coey, J.M.: Solid State Sci. **7**, 660 (2005)
2. Dutta, S., Chattopadhayay, S., Sarkar, A., Chakrabarthi, M., Sanyal, D., Jana, D.: Prog. in Mater. Science **54**, 89 (2009)
3. Lorenz, K., Alves, E., Wendler, E., Bilani, O., Wesch, W., Hayes, M.: Appl. Phys. Lett. **87**(191904), 1–3 (2005)
4. Watkins, G.D.: Phys. Solid State **41**(5), 746 (1999)
5. Pan, H., Yi, J.B., Shen, L., Wu, R.Q., Yang, J.H., Liu, J.Y., Feng, Y.P., Ding, J., Van, L.B., Yin, J.H.: Phys. Rev. Lett. **99**, 127–201 (2007)
6. Ziegler, J., Ziegler, M.D., Biersack, J.P. Nucl. Instrum. Meth. **B268**, 1818 (2010)
7. Gunnlaugsson, H.P., Mølholt, T.E., Mantovan, R., Masenda, H., Naidoo, D., Dlamini, W.B., Sielemann, R., Bharuth-Ram, K., Weyer, G., Johnston, K., Langouche, G., Ólafsson, S., Gíslason, H.P., Kobayashi, Y., Yoshida, Y., Fanciulli, M.: ISOLDE collaboration. Appl. Phys. Lett. **97**, 152–501 (2010)
8. Gunnlaugsson, H.P., Johnston, K., Molholt, T.E., Weyer, G., Mantovan, R., Masenda, H., Naidoo, D., Olafsson, S., Bharuth-Ram, K., Gislason, H.P., Langouche, G., Madsen, M.B.: ISOLDE collaboration. Appl. Phys. Lett. **100**, 042–109 (2012)
9. Weyer, G., Gunnlaugsson, H.P., Mantovan, R., Naidoo, D., Bharuth-Ram, K., Fanciulli, M., Agne, T.: J. Appl. Phys. **102**, 113915 (2007)
10. Molholt, T.E., Gunnlaugsson, H.P., Johnston, K., Mantovan, R., Masenda, H., Olafsson, S., Bharuth-Ram, K., Gislason, H.P., Langouche, G., Weyer, G.: Physica Scripta **T148**, 014–006 (2012)
11. Mantovan, R., Gunnlaugsson, H.P., Naidoo, D., Ólafsson, S., Mølholt, T.E., Johnston, K., Bharuth-Ram, K., Fanciulli, M., Langouche, G., Sielemann, R., Weyer, G., Gíslason, H.P., Madsen, M.B.: ISOLDE collaboration. J. Phys.: Condens. Matter **24**, 485–801 (2012)
12. Mantovan, R., Gunnlaugsson, H.P., Johnston, K., Masenda, H., Molholt, T.E., Naidoo, D., Ncube, M., Shayestehaminzadeh, S., Bharuth-Ram, K., Fanciulli, M., Gislason, H.P., Langouche, G., Olafsson, S., Perreira, L.M.C., Wahl, U., Torelli, P., Weyer, G.: Adv. Electron. Mater. **1**, 1400039 (2015)
13. Adekore, B.T., Davis, R.F., Barlage, D.W.: J. Appl. Phys. **101**, 024–902 (2007)
14. Borges, R.P., da Silva, R.C., Magalhaes, S., Cruz, M.M., Godinho, M.: J. Phys.: Condens. Matter **101**, 476–207 (2007)

15. Mishra, D.K., Singh, S.K., Kumar, P., Kanjilal, D., Sharma, M.K., Chatterjee, R., Srinivasu, V.V.: AIP Conf. Proc. **1276**, 388 (2010)
16. Anderson, J., Van de Walle, C.: Phys. Rev. B **76**, 165–202 (2008)
17. Zhou, S., Xu, Q., Potzger, K., Talut, G., Grötzshel, R., Fassbender, J., Vinnichenko, M., Grenzer, J., Helm, M., Hochmuth, H., Lorenz, M., Grundmann, M., Schmidt, H.: Appl. Phys. Lett. **93**, 232–507 (2008)
18. Subramanian, M., Akaike, Y., Hayashi, Y., Tanemura, M., Ebisu, H., Ping, D.L.S.: Phys. Status Solidi **244**, 1254 (2012)
19. Pham, A., Assadi, M.H.N., Zhang, Y.B., Yu, A.B., Li, S.: J. Appl. Phys. **110**, 123–971 (2011)